Resolution of mixtures of fluorophores in biological media using fluorescence spectroscopy and Monte Carlo simulation

Lyes Lakhal, Victor Acha, Thierry Aussenac

Resolution of mixtures of fluorophores in biological media using fluorescence spectroscopy and Monte Carlo simulation

Lyes Lakhal[a,*], Victor Acha[b], Thierry Aussenac[a]

[a]Institut Polytechnique LaSalle Beauvais, 19 rue Pierre Waguet, BP 30313, 60026 Beauvais, France

[b]Hydrogeochemistry and Soil-Environment Interactions (HydrISE) Unit, Institut Polytechnique LaSalle Beauvais, 19 rue Pierre Waguet, BP 30313, 60026 Beauvais, France

[*] Corresponding author. Tel.: + 33 (0)3 44 06 89 68; Fax: + 33 (0)3 44 06 25 26.

E-mail: lyes.lakhal@lasalle-beauvais.fr

Abstract

In excitation-emission fluorescence spectroscopy, the simultaneous quantitative prediction and qualitative resolution of mixtures of fluorophores using chemometrics is a major challenge because the scattering and reabsorption effects (turbidity) presented mainly in bio-materials. The measured fluorescence spectra are distorted by multiple scattering and reabsorption events in the surrounding medium, thereby diminishing the performance of the commonly used three-way resolution methods such as PARAllel FACtor (PARAFAC) analysis or Multivariate Curve Resolution–Alternating Least Squares (MCR–ALS).

In this work we show that spectral loadings and concentration profiles from model mixtures provided by PARAFAC and MCR-ALS are severely distorted by reabsorption and scattering phenomena although both models fit rather well the experimental data in terms of percentage of the explained variance.

The method to correct the fluorescence Excitation-Emission Matrix (EEM) consisted in measuring the optical properties (absorption parameter μ_a, scattering parameter μ_s, and anisotropy factor g) of samples and calculating the corresponding transfer function by means of the Monte Carlo simulation method. Applying this transfer functions to the measured EEM it was possible to compensate for reabsorption and scattering effects, and restore the ideal EEM, i.e., the EEM that is due only to fluorophores, without distortions from the absorbers and scatterers that are present. The PARAFAC and MCR-ALS decomposition of the resulting ideal EEMs provided spectral loadings and concentration profiles that matched the true profiles.

Key words: Fluorescence Spectroscopy; Reabsorption; Scattering; Monte Carlo; MCR-ALS; PARAFAC.

INTRODUCTION

Fluorescence spectroscopy is a fast, non-destructive technique with high sensitivity and selectivity providing quantitative and qualitative information in a wide variety of biological materials.[1-3] In fluorescence excitation-emission spectroscopy, a sample containing a mixture of fluorophores is excited by a beam of light at several wavelengths which causes it to emit light at different wavelengths, resulting in an excitation-emission matrix (EEM).[3] When several EEMs are measured the data can be arranged in a three-way array, $\underline{\mathbf{X}}$ ($I \times J \times K$), where $i = 1,\ldots, I$ represents the sample mode, $j = 1, \ldots, J$ the emission mode and $k = 1,\ldots, K$ represents the excitation mode. Note that, throughout this paper, scalars are shown in italics, vectors are bold lowercase letters, two-way matrices are bold uppercase letters, and three-way arrays are underscored bold uppercase letters.

Using curve resolution methods, it is possible under some circumstances, to perform the so-called mathematical chromatography; that is, to decompose the three-way array $\underline{\mathbf{X}}$ into the contributions from the underlying individual fluorophores. For each fluorophore, the pure excitation and emission spectra are obtained as well as the relative concentration. Among the existing algorithms, PARAFAC[4-6] and MCR-ALS[7-9] are most frequently mentioned in the literature. Assuming trilinearity, the PARAFAC decomposition factorizes the three-way array $\underline{\mathbf{X}}$ into a sum of finite series of tensor products of three vectors. A major advantage of data following this model is that the decomposition is unique,[10] permitting vectors associated with individual component of mixture (spectra, concentration profiles) to be extracted directly. The trilinearity hypothesis underlying PARAFAC implies that only the concentrations of fluorophores are allowed to change from one EEM to the other. The excitation and emission spectra on the other hand, should remain the same.

MCR-ALS method is capable of dealing with non-trilinear EEMs sharing only one order in common (either pure excitation or pure emission spectra). In MCR-ALS, the three-way array $\underline{\mathbf{X}}$ is first unfolded along the mode which breaks the trilinear structure to create an augmented matrix. This augmented matrix is then decomposed either by rows (excitation) or by columns (emission) according to a bilinear model. If the matrix is decomposed by columns, MCR-ALS would yield sets of emission profiles for each factor (one set for each EEM), and one set (common to all EEMs) of excitation profiles for each factor. If the matrix is decomposed by rows, MCR-ALS would yield one set of emission profiles for each factor and sets of excitation profiles for each factor (one set for each EEM). A single set of emission or excitation profiles may then be selected for comparison, or all recorded sets may be averaged to create one set of emission or excitation profiles. The intensity at each wavelength is then related to the concentration of each component in the mixture. However, if the data set is not trilinear, the solution provided by MCR-ALS method is not unique due to the presence of rotation ambiguities. Hence, constraints are essential to improve the quality of the final results and decrease the space of feasible solutions.[11]

Fluorescence spectra measured from biological samples are very often distorted due to reabsorption and scattering of the exciting light (known as primary inner filter effect) as well as the fluorescent light (known as secondary inner filter effect).[12] Additional dips or shoulders occur in the measured emission and excitation spectra at the position of absorption bands of natural chromophores such as hemoglobin in animal tissues or beta-carotene in fruit and vegetables. The inner-filter effect is immensely strong in the spectra from biological media because multiple scattering increases the path lengths of photons inside the sample.[13] In previous work,[14] fluorescence Monte Carlo model was used to simulate fluorescence data originating from mixtures of three known fluorophores

embedded in different absorbing and scattering environments. It has been shown that the fluorescence spectral information is severely altered by multiple scattering and reabsorption events in the surrounding medium, thereby preventing the consistent resolution and quantitative determination of the mixture by using multivariate data analysis methods such as PARAFAC and MCR-ALS. This is why fluorescence studies in undiluted biological samples require that inner filter effects be minimized or compensated for before a qualitative and quantitative analysis can be made.

Inner filter effects were studied for a long time now[15-17] and several models for correcting the fluorescence emission spectra for inner filter effects were proposed.[17-24] The formulation of these models assumes that the fluorescence spectra are measured in non-scattering media and the light intensity decreases exponentially along the axis of propagation. Unfortunately, these assumptions don't hold in the context of fluorescence spectroscopy of biological samples. The Monte Carlo stochastic method based on random walk of photons offers a flexible, yet rigorous approach to photon transport in absorbing and scattering media.[25]

In this paper, Monte Carlo based approach will be used to remove the aforementioned effects from the measured EEM and recover the ideal EEM. The starting point is that the measured EEM is theoretically related to the ideal EEM by a transfer function (TF) that accounts for the absorption and scattering properties of the medium. The TF of the sample is simulated by means of the Monte Carlo method on the basis of the optical properties of the medium (the absorption coefficient μ_a, the scattering coefficient μ_s, and the anisotropy factor g). These optical properties were calculated from integrating sphere measurements by using the inverse adding doubling software. The accuracy of the method will be tested on a laboratory-made fluorescence EEM data sets measured

from synthetic solutions of three fluorophores (Eosin Y, Fluorescein and Rhodamine B), an absorber (1,1′-Diethyl-2,2′-cyanine iodid) and a scatterer (Intralipid20%).

MATERIALS AND METHODS

Preparation of fluorescent synthetic solutions

Synthetic solutions mimicking the absorption, scattering and fluorescence properties of biological specimens were prepared using selected concentrations of Eosin Y (HT110280, Sigma-Aldrich), Fluorescein (46945, Sigma-Aldrich) and Rhodamine B (R6626, Sigma-Aldrich) as fluorophores, 1,1′-Diethyl-2,2′-cyanine iodide (323764, Sigma-Aldrich) as an absorber and Intralipid20% (I141-100ML, Sigma-Aldrich) as a source of scattering. Studies were carried out in ten solutions prepared in deionized water using different concentrations of fluorophores, 1,1′-Diethyl-2,2′-cyanine iodide, and fixed concentration of Intralipid20%, as listed in Table I. Notice that the absolute concentrations of fluorophores and absorber were chosen very low to fulfill the probability of more light scattering than light being absorbed like in real biological samples. 1,1′-Diethyl-2,2′-cyanine iodide is one of Cyanine dyes known for its cytotoxic effects and used as potential anticancer agents in the pharmaceutical sector. It is minimally fluorescent in the region between 300 and 650 nm[26, 27] and has absorption maxima at 490 and 525 nm. These peaks fall in the fluorescence excitation and emission wavelengths of the selected fluorophores. Intralipid20% is a standardized aqueous fat emulsion used for clinical applications as an intravenous nutrient.

In biomedical optics it is commonly used as a scattering medium to investigate light propagation in biological tissues.[28] The background absorption of diluted Intralipid20% is close to that of water

in which it is diluted in.[29] No traces of precipitation were noticed in the Intralipid20% solutions with fluorophores neither deterioration of solutions over time.

Determination of the optical properties

The absorption coefficient (μ_a), scattering coefficient (μ_s), and anisotropy factor (g) of samples were determined by applying the inverse-adding doubling (IAD) method to the measurements of total diffusive reflectance R_D, total diffusive transmittance T_D and collimated transmittance T_C.[30] All measurements were performed in the 300 to 700 nm range using a scanning. monochromator spectrophotometer (Evolution 600, Thermo Fisher Scientific, Madison, WI, USA). An average integration time of 0.4 s, a signal band width of 4.0 nm and a wavelength interval of 1.0 nm were applied in setting the photomultiplier tube (PMT) detector. Measurements with an integrating sphere set up were described earlier.[30,31]

Experimental values of R_D, T_D and T_C were input into the inverse-adding doubling program[32] to obtain the values of μ_a, μ_s, and g coefficients. The core of the IAD program consists of a numerical solution to the one-dimensional radiative transport equation (RTE)[33,34] which describes light propagation at steady state in a scattering medium, by means of the adding-doubling approach with a Henyey-Greenstein phase function.[32] Since this numerical solution of the RTE calculates the total reflectance R_T and the total transmittance T_T for a given set of optical properties, the Levenberg-Marquardt nonlinear least squares-fitting algorithm[35] has been used to find a set of feasible optical properties for which the calculated reflectance and transmittance values match the measured ones. The IAD software package can be freely downloaded from the Oregon Medical Laser Center web page (http://omlc.ogi.edu/).

Fluorescence measurements

A spectrofluorometer (Fluorolog 3, Model FL3-21, Jobin-Yvon Horiba, Longjumeau, France) was used to record fluorescence EEMs from synthetic solutions. The Fluorolog 3 was equipped with a 450 W Xenon short arc lamp source that was focused onto tunable, double excitation spectrometer (Czerny-Turner 1200/mm kinematic grating blazed at 330 nm) to produce a monochromatic collimated excitation beam at the sample at any desired wavelength from 290-900 nm. The remitted fluorescence was collected at 22.5° from the excitation direction, collimated, and dispersed by a tunable double emission spectrometer (Czerny-Turner 1200/mm kinematic grating blazed at 500 nm) into a multialkali photomultiplier tube detector. The system was interfaced to a computer via custom software (FluorEssence) that allowed an automated scanning of the sample. The sample was front illuminated to obtain the EEM for 17 excitation wavelengths between 320 and 400 nm while monitoring the emission between 354 - 584 nm (at 5 nm increments). The acquisition time of a single EEM was approximately 6 minutes.

Extraction of ideal fluorescence EEM

Under so-called "ideal" or optically dilute conditions, the fluorescence intensity $EEM_{IDEAL}(\lambda_k, \lambda_j)$ at particular excitation (λ_k) and emission (λ_j) wavelength due to F fluorophores is defined according to "Eq. 1":[14]

$$EEM_{IDEAL}(\lambda_k, \lambda_j) = \sum_{f=1}^{F} a_f b_f(\lambda_j) c_f(\lambda_k) \quad (1)$$

where a_f, $\mathbf{b_f}$ and $\mathbf{c_f}$ represent the relative concentration, the excitation spectrum and the emission spectrum of the f^{th} fluorophore, respectively.

Fluorescence in absorbing and scattering media consists of three components: the distribution of the excitation light in the medium which is a function of the optical parameters at the excitation wavelength λ_k; the fluorescence of isotropically radiating point sources located at different depths within the medium; and the total fluorescence escaping the medium surface which is a function of optical parameters at the emission wavelength λ_j. The measured or raw EEM $\mathbf{EEM_{RAW}}$ can be written as the product of the ideal EEM $\mathbf{EEM_{IDEAL}}$ and the transfer function **TF** which accounts for absorption and scattering effects:[14]

$$EEM_{RAW}(\lambda_k, \lambda_j) = EEM_{IDEAL}(\lambda_k, \lambda_j) \times TF(\lambda_k, \lambda_j) \quad (2)$$

This fundamental relation provides the key for linking the intrinsic fluorescence matrix which is independent of the sample's optical properties, $\mathbf{EEM_{IDEAL}}$, to the raw fluorescence matrix $\mathbf{EEM_{RAW}}$, depending on both the fluorophores and the sample's optical properties. "Equation 2" can be used to calculate $\mathbf{EEM_{IDEAL}}$ by dividing the observed fluorescence $\mathbf{EEM_{RAW}}$ by the transfer function matrix **TF**. Conventional PARAFAC and MCR-ALS methods can be then applied to the resulting data matrices.

The transfer function **TF** depends only on the sample optical parameters and is evaluated using the Fluorescence Monte Carlo program described earlier.[14]

Accuracy of the method: numerical simulations

There are two important sources of error that can influence the **TF** performance: errors related to the determination of optical parameters and those related to the noise of measurements. Although the noise is relatively small in steady state fluorescence spectroscopy, dividing this by the TF can significantly amplify this noise and particularly in the spectral regions where TF << 1 (with huge

absorbance regions). The impact of these two sources of error was evaluated through numerical simulations:

EEM_{IDEAL} of a mixture of three fluorophores was first simulated according to Eq. 1. Figure 1 shows the excitation and emission spectra of these three fluorophores and the corresponding **EEM_{IDEAL}.** Using the Monte Carlo method, $TF(\lambda_k, \lambda_j)$ of a turbid medium was then calculated. This simulated medium was characterized by its absorption parameter (μ_a), scattering parameter (μ_s) and anisotropy factor (g) (Figure 2). μ_a presents two typical peaks and varies from 0 cm^{-1} to 50 cm^{-1}, while μ_s and g are constants with values of 100 cm^{-1}, and 0.6, respectively. It should be noted that the absorption and scattering values used in this simulation are high compared to those observed in biological tissues[36].

The contaminated **EEM_{RAW}** by absorption and scattering effects was finally calculated by multiplying point by point **EEM_{IDEAL}** and **TF** (Eq. 2) (Figure 3).

In the determination of optical parameters error was introduced by varying the initial values of optical parameters simultaneously (Figure 2) from -40% (under estimation) to 40% (over estimation) by 5% increments:

$$\begin{cases} \mu_a^{err}(\lambda) = \left(1 + \frac{\Delta\mu_a}{\mu_a}\right)\mu_a(\lambda) \\ \mu_s^{err}(\lambda) = \left(1 + \frac{\Delta\mu_s}{\mu_s}\right)\mu_s(\lambda) \\ g^{err}(\lambda) = \left(1 + \frac{\Delta g}{g}\right)g(\lambda) \end{cases} \quad (3)$$

For each triplet $(\mu_a^{err}, \mu_s^{err}, g^{err})$ **TF** was simulated and applied to $\mathbf{EEM_{RAW}}$ to get $\mathbf{EEM_{IDEAL}^{ESTIM\_1}}$,

$$EEM_{IDEAL}^{ESTIM\_1}(\lambda_k, \lambda_j) = \frac{EEM_{RAW}(\lambda_k, \lambda_j)}{TF(\lambda_k, \lambda_j)} \quad (4)$$

The effects in the determination of optical parameters on the restoration quality of $\mathbf{EEM_{DIL}}$ were quantified by the term r_1 given by:

$$r_1[\%] = 100\frac{\sum_{k=1}^{N}\sum_{j=1}^{M}\left(EEM_{IDEAL}(\lambda_k,\lambda_j) - EEM_{IDEAL}^{ESTIM\_1}(\lambda_k,\lambda_j)\right)^2}{\sum_{i=1}^{N}\sum_{j=1}^{M}\left(EEM_{IDEAL}(\lambda_k,\lambda_j)\right)^2} \quad (5)$$

To quantify the influence of measurement noise:

- (a) $\mathbf{EEM_{RAW}}$ is contaminated with Gaussian noise of variance σ^2 and with zero mean:

$$EEM_{RAW}^{NOISY}(\lambda_k,\lambda_j) = EEM_{RAW}(\lambda_k,\lambda_j) + \sigma B(\lambda_k,\lambda_j) \quad (6)$$

$$\sigma = 10^{\left(\frac{-SNR}{20}\right)} \times \frac{\|\mathbf{EEM_{RAW}}\|_F}{\|\mathbf{B}\|_F} \quad (7)$$

where $\mathbf{B}$ is a matrix of same size as $\mathbf{EEM_{RAW}}$ whose elements are Gaussian random variables with zero mean and unit variance, SNR is the signal to noise ratio and $\|\ \ \|_{\mathbf{F}}$ denotes the Frobenius norm symbol.

- (b) $\mathbf{EEM_{RAW}^{NOISY}}$ was then divided by **TF** to get $\mathbf{EEM_{IDEAL}^{ESTIM\_2}}$, that is to say the ideal EEM estimated in presence of measurement noise:

$$EEM_{IDEAL}^{ESTIM\_2}(\lambda_k,\lambda_j) = \frac{EEM_{RAW}^{NOISY}(\lambda_k,\lambda_j)}{TF(\lambda_k,\lambda_j)} \quad (8)$$

The noise effect on the quality of restoration of EEM_{DIL} is quantified by the term r_2 given by:

$$r_2[\%] = 100\frac{\sum_{k=1}^{N}\sum_{j=1}^{M}\left(EEM_{IDEAL}(\lambda_k,\lambda_j) - EEM_{IDEAL}^{ESTIM\_2}(\lambda_k,\lambda_j)\right)^2}{\sum_{i=1}^{N}\sum_{j=1}^{M}\left(EEM_{IDEAL}(\lambda_k,\lambda_j)\right)^2} \quad (9)$$

Trilinear model

When several fluorophores (F) are present in weakly absorbing, dilute sample set, the fluorescence intensity can be described as a trilinear model:

$$F_{IDEAL}^{ijk} = \sum_{f=1}^{F} a_{if} b_{jf} c_{kf} + e_{ijk} \quad (10)$$

where F_{IDEAL}^{ijk} is the intensity of fluorescence for the sample *i* at emission wavelength *j* and excitation wavelength *k*. Parameter a_{if} is directly proportional to the true concentration of the component *f* in the i^{th} sample. A vector $\mathbf{b_f}$ of elements b_{jf} *(j = 1, 2, 3,…)* represents the true emission spectrum of component f, a vector $\mathbf{c_f}$ of elements c_{kf} (*k = 1, 2, 3,…*) denotes the true excitation spectrum of component *f*, and e_{ijk} accounts for a residual term.

Optical properties effect on trilinearity

In the previous paper[14], Monte Carlo simulations were run to simulate fluorescence EEM data sets in turbid media. Although higher values for the percentage of variance explained [Fit (%)] achieved by PARAFAC and MCR-ALS models, none of these two methods yielded satisfactory results for both spectral and sample (concentration) modes. This means that both algorithms successfully fund out the true underplaying causes of data variations but without any physical and chemical meaning. These results could be explained by the mechanism by which the optical properties of samples contribute to the turbid (raw) EEMs. This mechanism consists to introduce in "Eq. 3" three parameters; each of them depends only on one mode: the first parameter (a_{if}^{TF}) is concentration (sample) dependent, the second parameter (b_{jf}^{TF}) depends on the emission wavelength and the last

parameter (c_{kf}^{TF})depends on the excitation wavelength. Theoretically, the elements F_{RAW}^{ijk} of the k^{th} turbid EEM should be described by:

$$F_{RAW}^{ijk} = \sum_{f=1}^{F} a_{if} a_{if}^{TF} b_{jf} b_{jf}^{TF} c_{kf} c_{kf}^{TF} + e_{ijk} \quad (11)$$

In "Eq. 4", we can make the following substitutions: $a'_{if} = a_{if} a_{if}^{TF}$, $b'_{jf} = b_{jf} b_{jf}^{TF}$ and $c'_{kf} = c_{kf} c_{kf}^{TF}$. This leads to:

$$F_{RAW}^{ijk} = \sum_{f=1}^{F} a'_{if} b'_{jf} c'_{kf} + e_{ijk} \quad (12)$$

It is clear that this is a trilinear model and that is why both PARAFAC and MCR-ALS gave satisfactory results in terms of both percentage of variance explained Fit [%] and CORCONDIA. On the other hand, as can be seen from "Eq. 5", the elements a_{if}, b_{jf} and c_{kf} are multiplied respectively by bound variables (a_{if}^{TF}, a_{jf}^{TF} and c_{kf}^{TF}), which cannot be taken outside the sum. Then, the use of curve resolution methods based on bilinear or trilinear models leads necessarily to estimates of $\mathbf{a'_f}$, $\mathbf{b'_f}$ and $\mathbf{c'_f}$ instead of $\mathbf{a_f}$, $\mathbf{b_f}$, and $\mathbf{c_f}$. This is why PARAFAC and MCR-ALS models failed to provide pure-analyte profiles.

It is worth noting that in the particular case where the two variables b_{jf}^{TF} and c_{kf}^{TF} are fluorophore-independent variables, "Eq. 5" corresponds exactly to the ideal trilinear model for fluorescence EEMs in the presence of quenching proposed by Wentzell et al.[37]

Multiway Analysis of Fluorescence Data

The reference, raw and ideal EEMs were grouped in three three-way data sets A, B and C, respectively, containing each 25 excitation wavelengths, 44 emission wavelengths and 10 samples.

PARAFAC and MCR-ALS methods were then used to decompose the datasets into several spectral profiles of the contributing components. The recovery of relative concentration and spectral profiles was assessed by the relative residual sum of squares (*RRSS*):

$$RRSS = 100 \times \frac{\sum_i \left(x_i^{calc} - x_i^{true}\right)^2}{\sum_i (x_i^{true})^2} \quad (13)$$

Where $\mathbf{x}^{\mathbf{calc}}$ and $\mathbf{x}^{\mathbf{true}}$ are respectively the response profile calculated with PARAFAC or MCR-ALS, and the true response profile. The lower the value of the RRSS term is, the closer the calculated profile is to the true response.

PARAFAC modeling was carried out using the N-way Toolbox for MATLAB.[38] A convergence criterion of 1×10^{-6} (default in the algorithm) and a maximum number of iterations of 2500 were chosen. The unconstrained models were chosen because an attempt to fit a PARAFAC models with non-negativity constraints in the spectral mode resulted in no significant improvement compared to the unconstrained option (data not shown). MCR-ALS analysis was carried out with software currently available in the MCR-ALS home page (http://www.ub.edu/mcr/welcome.html). The MCR-ALS decomposition was done using non-negativity constraints for both spectral modes performed with the fast non-negative least- squares algorithm. The structure of the reference and estimated ideal EEMs was assumed trilinear while a non-trilinear structure was selected for the MCR-ALS decomposition of the raw EEMs. The matrix of emission profiles provided by PARAFAC model was taken as the initial estimate for emission spectra.

The MCR-ALS procedure decomposes an unfolded fluorescence three-way array into two matrices: one matrix containing the excitation spectra as a function of the sample index k (here $1 \leq k \leq 10$), and the second matrix containing the emission spectra which are common to all samples. Thus for clarity reasons only the excitation spectra corresponding to the first sample (the less

affected by absorption and scattering effects) will be shown later on. The MCR-ALS relative concentration profiles are given by the maximum peak value of each one of the excitation spectra. Before decomposing the EEM data sets, the underlying number of factors was estimated according to the percentage of the explained variance [*Fit (%)*] and CORe CONsistency DIAgnosis [*CORCONDIA*].[39] Results shown in Table II indicate that 3 factors are suitable for the EEM PARAFAC decomposition.

RESULTS AND DISCUSSION

Simulation results

Figure 4 shows the evolution of $r_1[\%]$ based on the relative error on the determination of optical parameters. As we can see, the term r_1 is relatively stable, it increased by only 10% when the error on each one of the three parameters is 40%, which corresponds to a ratio of 0.25. This result demonstrates that the Monte Carlo based TF is stable regarding the uncertainties on the determination of optical parameters.

Figure 5 shows $\mathrm{EEM}_{\mathrm{IDEAL}}^{\mathrm{ESTIM\_2}}$ for some values of SNR. As can be seen the division by TF does not introduce a drastic amplification of the measurement noise even in regions of strong absorption.

Figure 6 shows the evolution of r_2 term as a function of SNR. The value of r_2 falls from 28% to less than 1% when the SNR increases from 5 dB to 25 dB. For *SNR* values greater than 25 dB, values generally obtained in steady state fluorescence spectroscopy of biological media, r_2 values become irrelevant. This result demonstrates the robustness of TF with respect to the noise of measurement.

Recovery of the ideal EEM (EEM_{IDEAL}) from measured EEM (EEM_{RAW})

Figure 7 shows the representative raw EEM $\mathbf{EEM_{RAW}}$, the simulated transfer function **TF**, the reference EEM $\mathbf{EEM_{REF}}$ (first row) and the ideal EEM $\mathbf{EEM_{IDEAL}}$ for model solution 1 (Table I), model solution 5 (second row) and for model solution 10 (third row) in the form of contour plots. $\mathbf{EEM_{REF}}$ was measured for each solution from the corresponding pure solution, i.e. the solution that contains the same mixture of fluorophores (Eosin Y, Fluorescein and Rhodamine), without the absorber (1,1′-Diethyl-2,2′-cyanine iodide), and without the scatter (Intralipid20%). All figures were plotted on a log scale for clarity.

The impact of the **TF**, i.e. the optical properties, is clearly visible on the raw EEM $\mathbf{EEM_{RAW}}$. One can observe severe deformations of the line shapes (contours) and the appearance of a dip at around 520 nm excitation wavelength, which is due to 1,1′-Diethyl-2,2′-cyanine iodide absorption peak. When the absorption becomes stronger (high concentration of 1,1 '-Diethyl-2, 2'-cyanine iodide) this dip gave rise to a fluorescence peak at wavelength pair (λ_k = 508 nm, λ_j = 570 nm).

The ideal EEM $\mathbf{EEM_{IDEAL}}$ was calculated from dividing the raw EEM $\mathbf{EEM_{RAW}}$ by the **TF**. A good agreement was observed in comparing $\mathbf{EEM_{IDEAL}}$ to $\mathbf{EEM_{REF}}$. The two EEMs share the same features and the contour plots practically match. In comparing the $\mathbf{EEM_{RAW}}$ and $\mathbf{EEM_{IDEAL}}$, the most obvious change was the disappearance of the fluorescence peak at wavelength pair (λ_k = 508 nm, λ_j = 570 nm) in the calculated $\mathbf{EEM_{IDEAL}}$. In addition, the dip shown in the $\mathbf{EEM_{RAW}}$ at around 520 nm, which is due to 1,1 '-Diethyl-2, 2'-cyanine iodide absorption, was also corrected in the calculated $\mathbf{EEM_{IDEAL}}$.

PARAFAC and MCR-ALS loadings

The results obtained from the three-component PARAFAC and MCR-ALS models fitted to the data set A (Reference EEMs) are shown in Figure 8. The pure profiles were also plotted for comparison. The spectral profiles of the three components retrieved by PARAFAC and MCR-ALS are perfectly representative of the analytes in the model solutions (Figure 8). Component C_1 corresponds to Eosin Y, component C_2 to Fluorescein and component C_3 to Rhodamine B. The relative concentration profiles estimated by the two algorithms were close to the mixing proportions of the three fluorophores. The values of the RRSS terms were insignificant for all three fluorophores (Table III). These results confirm that the solutions were properly prepared and that the inner structure of the data set A is perfectly trilinear.

The results obtained by three-component PARAFAC and MCR-ALS models fitted to the data set B (raw EEMs) are shown in Table IV and Figure 9. According to the RRSS terms values listed in Table IV the solutions provided by MCR-ALS model were clearly better than those from PARAFAC model. This could be explained by the higher similarity of MCR-ALS underlying model to the real variation in the data set as stated by de Juan and Tauler.[9] However, the MCR-ALS recovered profiles remained far from the true profiles (Figure 9).

Figure 10 shows the results of four-component PARAFAC and MCR-ALS models fitted to the data set B (raw EEMs). Comparing these results to the three-component models (see Figure 9), the first three components have similar profiles; however, the fourth component has no chemical meaning. This fact confirms that the absorption and scattering effects cannot be compensated or eliminated by adding more components to the PARAFAC or MCR-ALS models.

These results confirm the conclusions obtained with the simulated data reported in previous paper[14] and briefly remembered in the beginning of the present paper (see Optical properties effect sub-section).

Figure 11 shows the profiles retrieved by three-component PARAFAC and MCR-ALS models for data set C (ideal EEMs). For spectral modes, the recovered profiles are remarkably similar to the pure profiles allowing the three fluorophores to be identified easily. For the sample mode, the trend in the estimations of the relative concentrations followed rather well the true relative concentrations of samples considering the different possible sources of error. Especially the Rhodamine B estimations were very close to the true values, whereas the Fluorescein estimations differed the most (Table IV). Obviously, this difference is related to the fact that the recovered concentration profile of Fluorescein is the most influenced by the absorption and scattering effects and Rhodamine B the least (see Table III).

Finally, in terms of performance, PARAFAC gave slightly better results than MCR-ALS (Table V). The reason is probably the uniqueness of the solutions obtained and relaxation of some constraints which were not applied in PARAFAC.

Comparison with existing methods

As mentioned earlier, several methods have been developed to avoid inner filter effects from fluorescence emission spectra[17-24]. However, the performances of these methods cannot be compared to those of our method for two reasons. The first reason is of technical order. The existing methods are based on measurements which are not possible to perform in turbid media such as biological media. To perform corrections these methods use either the sample's absorbance[17-22], the EEM of the sample twice diluted[23] or the 1st order Raman scatter peak contained in the

measured fluorescence emission spectra[24]. The measurements of sample's absorbance, and the twice diluted methods are very easy to achieve in a dissolved organic matter solution[23], however such measurements have no meaning in the case of a solid sample such as an animal tissue or a food product. On the other hand, we need also to consider the fact that most biological samples exhibit strong fluorescence emission in the spectral Raman region, which often swamps the relatively weak Raman signals. The second reason emerges from the mathematical model of fluorescent light propagation. The methods mentioned above assume that fluorescence spectra are measured in pure absorbing (non-scattering) samples where the intensity of fluorescence light (excitation light and emitted light) decreases exponentially along the axis of propagation. Unfortunately, these assumptions don't hold in the context of fluorescence spectroscopy of biological samples. After propagating over a few hundred micrometers, fluorescence light would become highly diffusive. Monte Carlo simulation is the only technique that accurately traces photon paths and gives an accurate estimation for light propagation in turbid media.

CONCLUSION

Reabsorption and scattering phenomena in turbid samples such as biological specimens severely deform their EEMs data while preserving their trilinear structure. The application of chemometric methods assuming a trilinear structure which is the case of PARAFAC or bilinear structure which is the case of MCR-ALS gives effectively good results in terms of percentage of explained variance; however these results have no chemical meaning. This could mislead the analyst when dealing with data sets from complex biological specimens containing multiple unknown components in the sense that the percentage of explained variance is used as criterion to determine

the inner structure of data sets, and allows to determine afterwards which family of data analysis (PARAFAC or MCR-ALS) methods is most appropriate to deal with.

Depending on the spectral localization of the fluorophore in the transfer function spectral plane, the effects of scattering and reabsorption can affect more or less severely the three modes (excitation, emission, and sample mode) of the same fluorophore, and for a given mode the distortion can be severe for one fluorophore and moderate or even insignificant for another fluorophore.

To eliminate the effects of scattering and reabsorption the Monte Carlo based approach was experimentally tested in model mixtures containing three fluorophores (Eosin Y, Fluorescein and Rhodamine) with controlled absorption and scattering properties imitating the optical properties of biological media. For each sample, the optical parameters were obtained from integrating sphere measurements and inverse adding doubling algorithm. The ideal EEM was accurately recovered from the measured EEM by dividing it by the wavelength-dependent transfer function which was simulated on the basis of the determined optical parameters. PARAFAC and MCR-ALS decompositions of the recovered ideal EEMs provided spectral and relative concentration profiles similar to the true profiles.

Synthetic mixtures of up to three fluorophores embedded in absorbing and scattering solutions were examined in this study. Although this method could accurately recover the ideal EEMs and extract the pure-analyte contributions from a mixture, there is an important limitation associated with it. This method uses the optical parameters of samples which are measured separately using an integrating sphere set-up. A future work would be done to improve this method for online setting, where the integrating sphere measurements may often be impractical.

REFERENCES

1. G.M. Escandar, N.M. Faber, H.C. Goicoechea, A. Muñoz de la Peña, A.C. Olivieri, R.J. Poppi. "Second and third-order multivariate calibration: Data, algorithms and applications". Trends Anal. Chem. 2007. 26 (7) : 752-765.
2. R. Bro. "Review on multiway analysis in chemistry 2000–2005". Crit. Rev. Anal. Chem. 2006. 36 (3-4): 279-293.
3. J. Christensen, L. Nørgaard, R. Bro, S.B. Engelsen. "Multivariate autofluorescence of intact food systems". Chem. Rev. 2006. 106 (6): 1979-1994.
4. J.D. Carroll, J. Chang. "Analysis of individual differences in multidimensional scaling via an N-way generalization of Eckart-Young decomposition". Psychometrika. 1970. 35 (3): 283-319.
5. R.A. Harshman. "Foundations on the PARAFAC procedure: model and conditions for an explanatory multimode factor analysis". UCLA Working Paper Phonetics. 1970. 16: 1-84.
6. R. Bro. "PARAFAC. Tutorial and applications". Chemom. Intell. Lab. Syst. 1997. 38 (2): 149-71.
7. R. Tauler. "Multivariate curve resolution applied to second order data". Chemom. Intell. Lab. Syst. 1995. 30 (1): 133-146.
8. R. Tauler, A.K. Smilde, B.R. Kowalski. "Selectivity, local rank, 3-way data analysis and ambiguity in multivariate curve resolution". J. Chemometr. 1995. 9 (1): 31-58.
9. A. de Juan, R. Tauler. "Chemometrics applied to unravel multicomponent processes and mixtures. Revisiting latest trends in multivariate resolution". Anal. Chim. Acta. 2003. 500 (1-2): 195–210.

10. L. De Lathauwer. “A Link between the Canonical Decomposition in Multilinear Algebra and Simultaneous Matrix Diagonalization”. SIAM. J. Matrix. Anal. Appl. 2006. 28 (3): 642-66.
11. H. Abdollahi, R. Tauler. “Uniqueness and rotation ambiguities in Multivariate Curve Resolution methods”. Chemom. Intell. Lab. Syst. 2011. 108 (2): 100-111.
12. J.R. Lakowicz. Principles of Fluorescence Spectroscopy. New York: Plenum Press, 1999. 2nd ed.
13. N. N. Zhadin, R. R. Alfano. “Correction Of The Internal Absorption Effect In Fluorescence Emission And Excitation Spectra From Absorbing And Highly Scattering Media: Theory And Experiment”. J. Biomed. Opt. 1998. 3 (2): 171-186.
14. L. Lakhal, V. Acha, T. Aussenac. “PARAFAC analysis of front-face fluorescence data: Absorption and scattering effects assessed by means of Monte Carlo simulations”. Chemom. Intell. Lab. Syst. 2012. 116 (?): 112-122.
15. J.L. Lauer. “Correction for light absorption in fluorescence and light scattering measurements”. J. Opt. Soc. Am. 1951. 41 (7): 482-483.
16. H. Braunsberg, S. B. Osborn. “Some general aspects of fluorimetric determinations”. Anal. Chim. Acta. 1952. 6: 84-95.
17. C.A. Parker, W.J. Barnes. “Some experiments with spectrofluorimeters and filter fluorimeters”. The Analyst. 1957. 82 (978): 606-618.
18. J. F. Holland, R.E. Teets, P.M. Kelly, A. Timnick. “Correction of right-angle fluorescence measurements for the absorption of excitation radiation”. Anal. Chem. 1977. 49 (6): 706-710.
19. S.A. Tucker, V.L. Amszi, W.E. Acree. “Primary and secondary inner filtering, Effect of $K_2Cr_2O_7$ on fluorescence emission intensities of quinine sulfate”. J. Chem. Educ. 1992. 69 (1): A8.

20. M. C. Yappert, J. D. Ingle. “Correction of Polychromatic Luminescence Signals for Inner-Filter Effects”. Appl. Spectrosc. 1989. 43 (5): 759-767.

21. A. Credi, P. Luca. “From observed to corrected luminescence intensity of solution systems: an easy-to-apply correction method for standard spectrofluorimeters”. Spectrochim. Acta, Part A. 1998. 54 (1): 159-170.

22. Q. Gu, J.E. Kenny. “Improvement of Inner Filter Effect Correction Based on Determination of Effective Geometric Parameters Using a Conventional Fluorimeter”. Anal. Chem. 2009. 81 (1): 420-426.

23. X. Luciani, S. Mounier, R. Redon, A. Bois. “A simple correction method of inner filter effects affecting FEEM and its application to the PARAFAC decomposition”. Chemom. Intell. Lab. Syst. 2009. 96 (2): 227-238.

24. T. Larsson, M. Wedborg, D. Turner. “Correction of inner-filter effect in fluorescence excitation-emission matrix spectrometry using Raman scatter”. Anal. Chim. Acta. 2007. 583 (2): 357-363.

25. L. V. Wang, H. Wu. Biomedical Optics: Principles and Imaging. Hoboken, NJ: Wiley, 2007.

26. E. Delaey, F. Van Laar, D. De Vos, A. Kamuhabwa, P. Jacobs, P. De Witte. “A comparative study of the photosensitizing characteristics of some cyanine dyes”. J. Photochem. Photobiol. B. 2000. 55 (1): 27-36.

27. C.J. Tredwell, C.M. Keary. “Picosecond time resolved fluorescence lifetimes of the polymethine and related dyes”. Chem. Phys. 1979. 43 (3): 307-316.

28. H.G. van Staveren, C.J.M. Moes, J. van Marle, S.A. Prahl, M.J.C. van Gemert. “Light scattering in Intralipid20% in the wavelength range of 400-1100 nanometers”. Appl. Opt. 1991. 30 (31): 4507-4514.

29. S.T. Flock, S.L Jacques, B.C. Wilson, W.M Star, M.J.C van Gemert. “Optical Properties of Intralipid: A phantom medium for light propagation studies”. Laser. Surg. Med. 1992. 12 (5): 510-519.

30. M.A. Velazco-Roa, and S.N. Thennadil. “Estimation of complex refractive index of polydisperse particulate systems from multiple-scattered ultraviolet-visible-near-infrared measurements”. Appl. Opt. 2007. 46 (18): 3730-3735.

31. E. Dzhongova. Monitoring Bacterial Growth in Liquid Cultures through the Bulk Optical Parameters in the Near-Infrared Region extracted using the Radiative Transfer Theory. [PhD. Dissertation] Newcastle: School of Chemical Engineering and Advanced Materials, University of Newcastle, 2010.

32. S.A. Prahl, M.J.C. van Gemert, A.J. Welch. “Determining the optical properties of turbid media by using the adding-doubling method”. Appl. Opt. 1993. 32 (4): 559-568.

33. S. Chandrasekhar. Radiative Transfer. New York: Dover Publications Inc, 1960.

34. I. Ishimaru. Wave Propagation and Scattering in Random Media. New York: Academic Press, 1978.

35. W.H. Press, S.A. Tuekolsky, W.T. Vettering, B.P. Flannery. Numerical Recipes in C: The Art of Scientific Computing. Cambridge, UK: Cambridge University Press, 1992. 2nd ed.

36. W.F. Cheong, S.A. Prahl, A.J. Welch. “A review of the optical properties of biological tissues”, IEEE. J. Quantum. Electron. 1990. 26 (12): 2166-2185.

37. P.D. Wentzell, S.S. Nair, R.D. Guy. “Three-Way Analysis of Fluorescence Spectra of Polycyclic Aromatic Hydrocarbons with Quenching by Nitromethane”. Anal. Chem. 2001. 73 (7): 1408-1415.

38. C.A. Andersson, R. Bro. “The N-way toolbox for MATLAB”. Chemom. Intell. Lab. Syst. 2000. 52 (1): 1-4.

39. R. Bro R, H.A.L. Kiers. “A new efficient method to determining the number of components in PARAFAC models”. J. Chemometr. 2003. 17 (5): 274–286.

Captions for figures

Figure 1: Simulated (a) excitation spectra, (b) emission spectra, and (c) $\mathbf{EEM_{IDEAL}}$ calculated from Eq. 1 for three fluorophores .

Figure 2: Optical parameters and simulated TF by using the Monte Carlo method. (a) absorption parameter μ_a, (b) scattering parameter μ_s, (c) anisotropy factor g, **(**d) Simulated **TF**.

Figure 3: $\mathbf{EEM_{RAW}}$ calculated from Eq. 2 by using $\mathbf{EEM_{IDEAL}}$ from Figure 1 and **TF** from Figure 2D.

Figure 4: Evolution of $r_1(\%)$ as a function of errors on the determination of optical parameters.

Figure 5: $\mathbf{EEM_{IDEAL}^{ESTIM\_2}}$ for *SNR* = 10 dB, *SNR* = 20 dB and *SNR* = 30 dB.

Figure 6: Evolution of $r_2(\%)$ ratio as a function of *SNR*.

Figure 7: Contour plots of raw EEM $\mathbf{EEM_{RAW}}$ (first column), simulated transfer function **TF (**second column), ideal EEM $\mathbf{EEM_{IDEAL}}$ (third column) and reference EEM $\mathbf{EEM_{REF}}$ (fourth column) for model solutions 1 (first row), 5 (second row) and 10 (third row) respectively (see Table I). The vertical dashed line at λ_k = 520 nm in the $\mathbf{EEM_{RAW}}$ of model solutions 5 and 10 indicates the dip introduced by the TF giving rise to a secondary fluorescence peak at wavelength pair (λ_k = 508 nm, λ_j = 570 nm).

Figure 8: Comparison of three-factor PARAFAC decomposition (dotted lines) and MCR-ALS (dashed lines) models of data set A (Reference EEMs) with pure profiles (solid lines) from three components (C_1-C_3). The pure excitation and emission spectra of each fluorophore were measured from the corresponding diluted standard solution. The spectral loadings are normalized by the maximum (maximum unity) and the concentration profiles (score loadings) are normalized by the

sum (sum unity). The concentration profiles represent thus the mixing proportions of the three fluorophores. Identification of components C_1-C_3 is given in the title of the upper subplots.

Figure 9: Comparison of three-component PARAFAC (dotted lines) and MCR-ALS (dashed lines) models of the data set B (raw EEMs) with true profiles (solid lines) from three components (C_1-$C_{3)}$. The spectral loadings are normalized by the maximum (maximum unity) and the concentration profiles (score loadings) are normalized by the sum (sum unity). The concentration profiles represent thus the mixing proportions of the three fluorophores. Identification of components C_1-C_3 is given in the title of the upper subplots.

Figure 10: Comparison of four-component PARAFAC (dotted lines) and MCR-ALS (dashed lines) models of data set B (raw EEMs) with true profiles (solid lines) from three components (C_1-$C_{3)}$. The spectral loadings are normalized by the maximum (maximum unity) and the concentration profiles (score loadings) are normalized by the sum (sum unity). The concentration profiles represent thus the mixing proportions of the three fluorophores. Identification of components C_1-C_3 is given in the title of the upper subplots.

Figure 11: Comparison of three-component PARAFAC (dotted lines) and MCR-ALS (dashed lines) models of data set C (ideal EEMs) with true profiles (solid lines) from three components (C_1-$C_{3)}$. The spectral loadings are normalized by the maximum (maximum unity) and the concentration profiles (score loadings) are normalized by the sum (sum unity). The concentration profiles represent thus the mixing proportions of the three fluorophores. Identification of components C_1-C_3 is given in the title of the upper subplots.

Table I: Composition of ten model solutions used for pointing out experimentally the absorption and scattering effects on fluorescence spectra of biological media.

Solution	Eosin Y (μM)	FITC (μM)	Rhodamine B (μM)	1,1′-Diethyl-2,2′-cyanine iodide (mg/L)	Intralipid20% (mL/L)
1	1.00	0	0	5.00	55.00
2	0.72	0.21	0.07	15.56	55.00
3	0.51	0.28	0.21	26.11	55.00
4	0.37	0.27	0.36	36.67	55.00
5	0.26	0.23	0.50	47.22	55.00
6	0.19	0.19	0.62	57.78	55.00
7	0.14	0.15	0.72	68.33	55.00
8	0.10	0.11	0.79	78.89	55.00
9	0.07	0.09	0.84	89.44	55.00
10	0.05	0.06	0.89	100.00	55.00

Table II: Decomposition of EEM data sets. Percentage of explained variance Fit [%] and CORCONDIA values from PARAFAC model as a function of the number of factors.

Number of factors	1	2	3	4	5	6	7
Data set A (reference EEMs)							
Fit [%]	90,40	98,91	99,96	99,97	99,97	99,97	99,97
CORCONDIA [%]	100,00	100,00	97,48	0,64	0,20	0,06	0,02
Data set B (raw EEMs)							
Fit [%]	87,39	98,94	99,75	99,79	99,83	99,84	99,85
CORCONDIA [%]	100,00	100,00	94,49	31,03	2,14	0,23	0,19
Data set C (ideal EEMs)							
Fit [%]	90,70	99,07	99,97	99,97	99,97	99,97	99,97
CORCONDIA [%]	100,00	100,00	98,51	12,75	-0,03	-0,08	0,09

Table III: Relative residual sum of squares (RRSS) terms obtained from PARAFAC and MCR-ALS models for data set A (reference EEMs).

Model	Mode	RRSS term [%]		
		Eosin Y	Fluorescein	Rhodamine B
PARAFAC	Excitation mode	0,29	0.72	0.14
	Emission mode	0,10	0.05	0.79
	Sample mode	0,60	0.70	0.32
MCR-ALS	Excitation mode	0,28	1.52	0.18
	Emission mode	0,10	0.05	0.81
	Sample mode	0,59	0.69	0.32

Table IV: Relative residual sum of squares (RRSS) terms obtained from PARAFAC and MCR-ALS models for data set B (raw EEMs).

Model	Mode	RRSS term [%]		
		Eosin Y	Fluorescein	Rhodamine B
PARAFAC	Excitation mode	13,26	86,07	38,33
	Emission mode	7,70	41,91	14,59
	Sample mode	97,31	368,00	5,16
MCR-ALS	Excitation mode	1,14	26,64	23,98
	Emission mode	6,12	40,73	14,84
	Sample mode	23,37	65,12	2,45

Table V: Relative residual sum of squares (RRSS) terms obtained from PARAFAC and MCR-ALS models for data set C (ideal EEMs).

Model	Mode	RRSS term [%]		
		Eosin Y	Fluorescein	Rhodamine B
PARAFAC	Excitation mode	0,32	3,92	2,41
	Emission mode	0,41	1,92	2,36
	Sample mode	2,91	8,43	0,30
MCR-ALS	Excitation mode	0,33	0,42	4,85
	Emission mode	0,40	2,09	2,33
	Sample mode	2,97	10,47	0,31

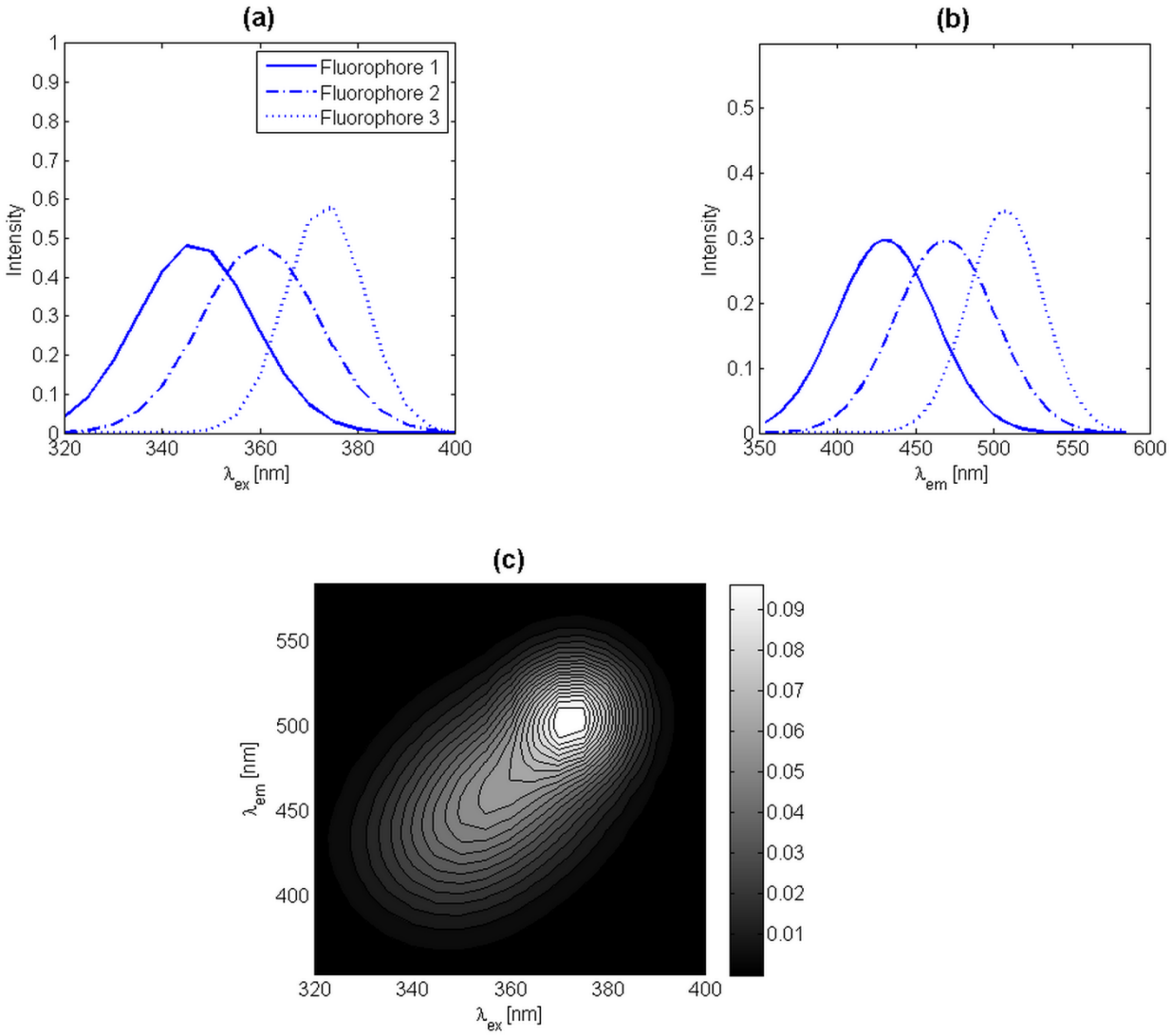
(a)
Fluorophore 1
Fluorophore 2
Fluorophore 3
Intensity
λex [nm]
(b)
Intensity
λem [nm]
(c)
λem [nm]
λex [nm]

Figure 1

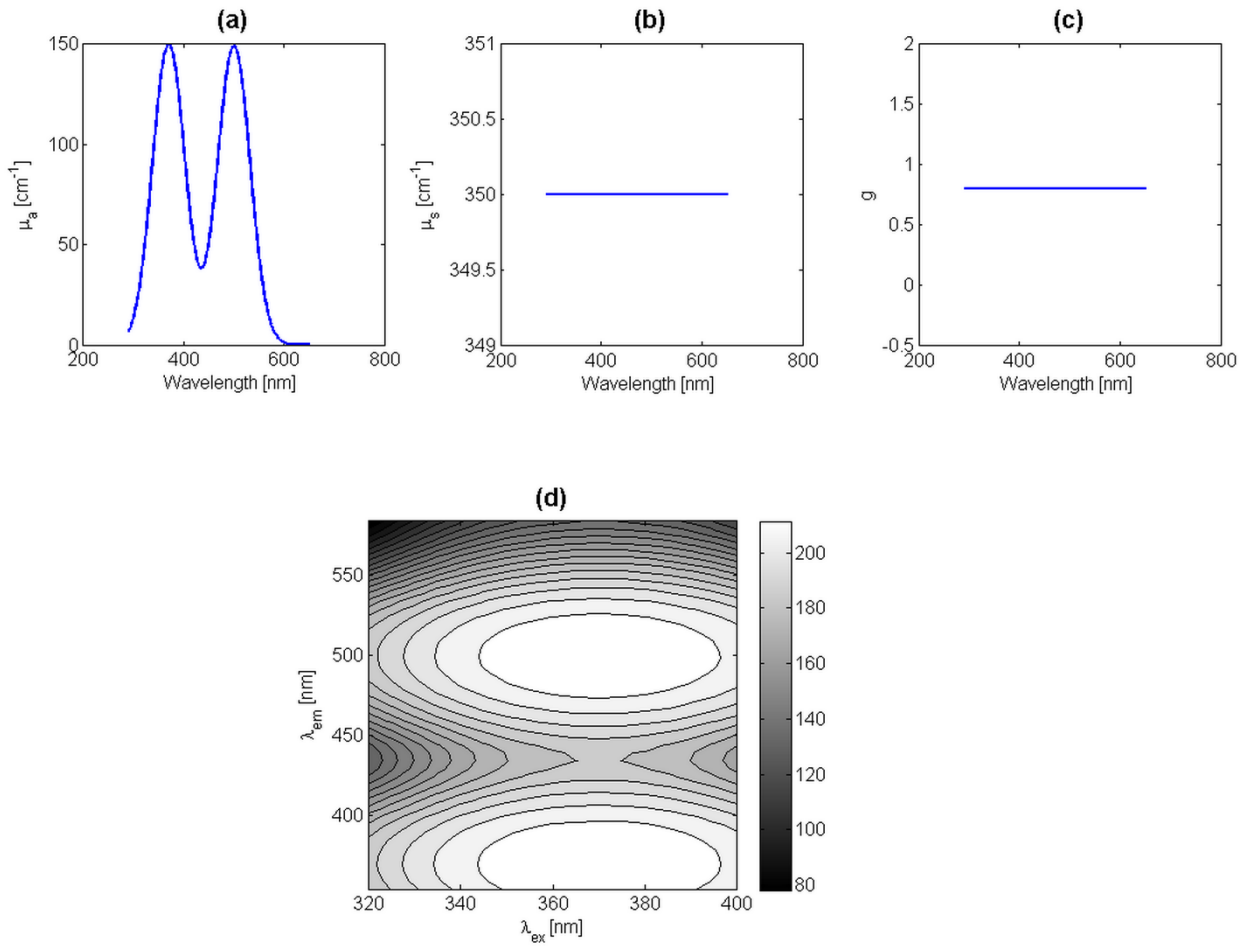
(a)
150
100
50
0
200
400
600
800
μ_a [cm^{-1}]
Wavelength [nm]
(b)
351
350.5
350
349.5
349
200
400
600
800
μ_s [cm^{-1}]
Wavelength [nm]
(c)
2
1.5
1
0.5
0
-0.5
200
400
600
800
g
Wavelength [nm]
(d)
550
500
450
400
320
340
360
380
400
λ_{em} [nm]
λ_{ex} [nm]
200
180
160
140
120
100
80

Figure 2

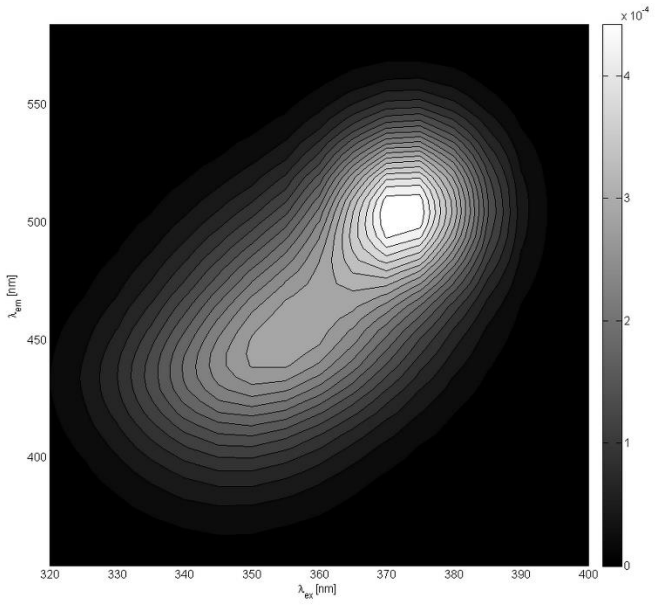
x 10^-4
4
3
2
1
0
550
500
450
400
λem [nm]
320
330
340
350
360
370
380
390
400
λex [nm]

Figure 3

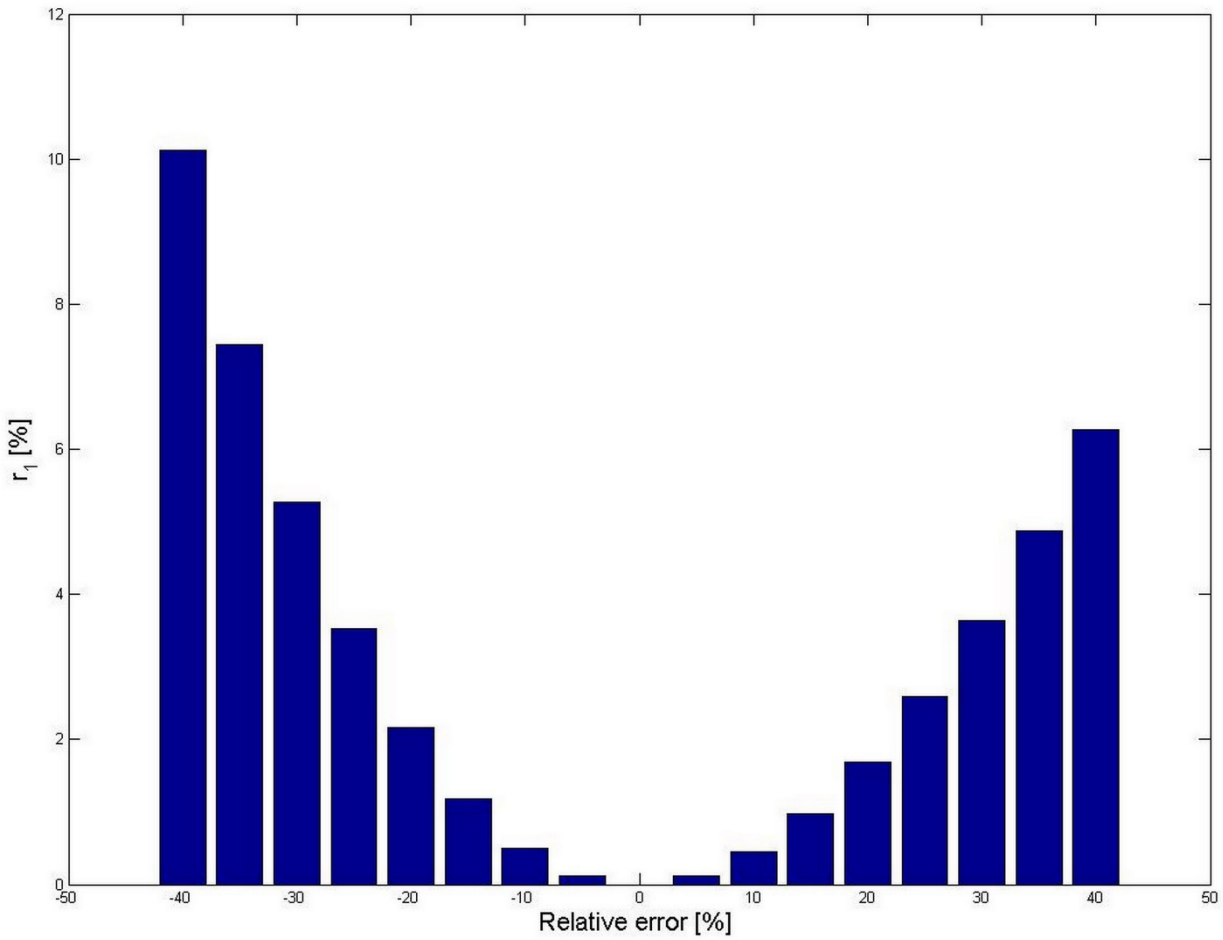

Figure 4

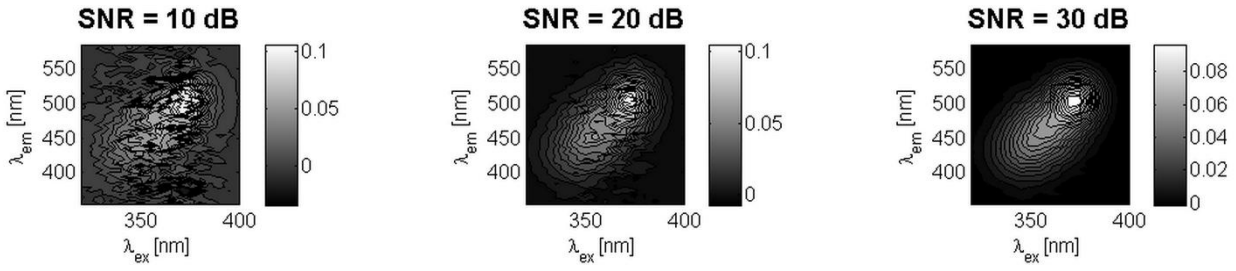

Figure 5

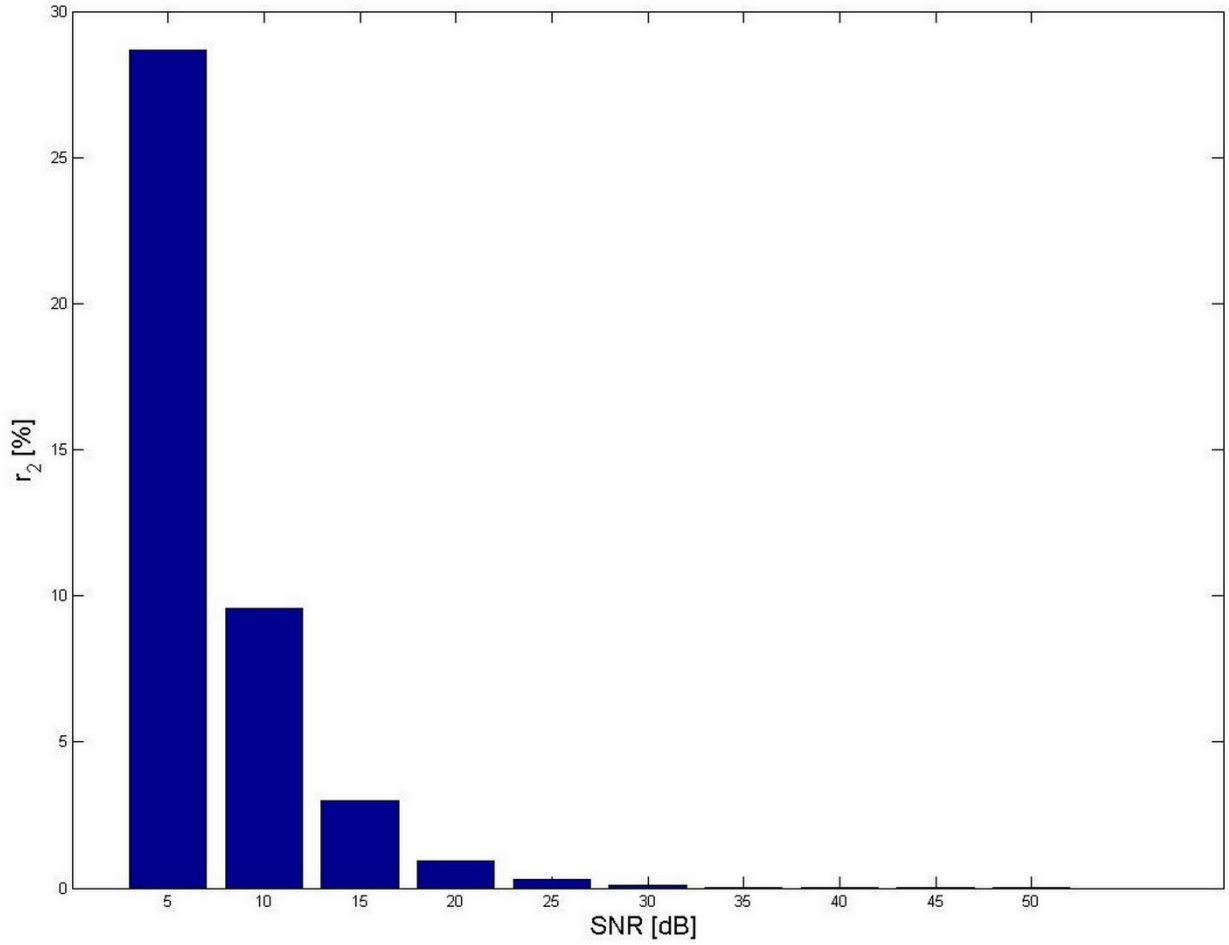

Figure 6

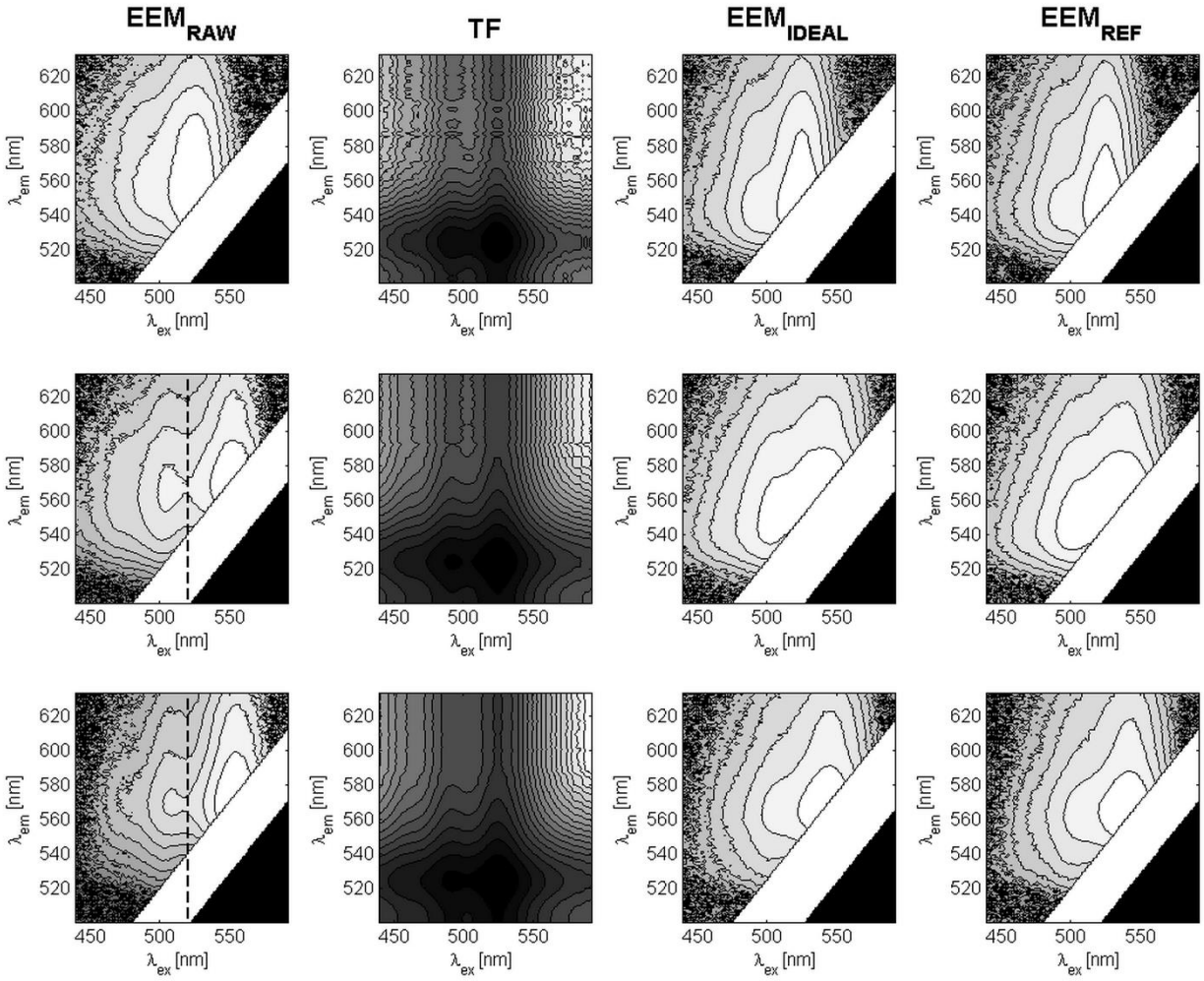
EEM RAW
TF
EEM IDEAL
EEM REF
λem [nm]
λex [nm]
620
600
580
560
540
520
450
500
550

Figure 7

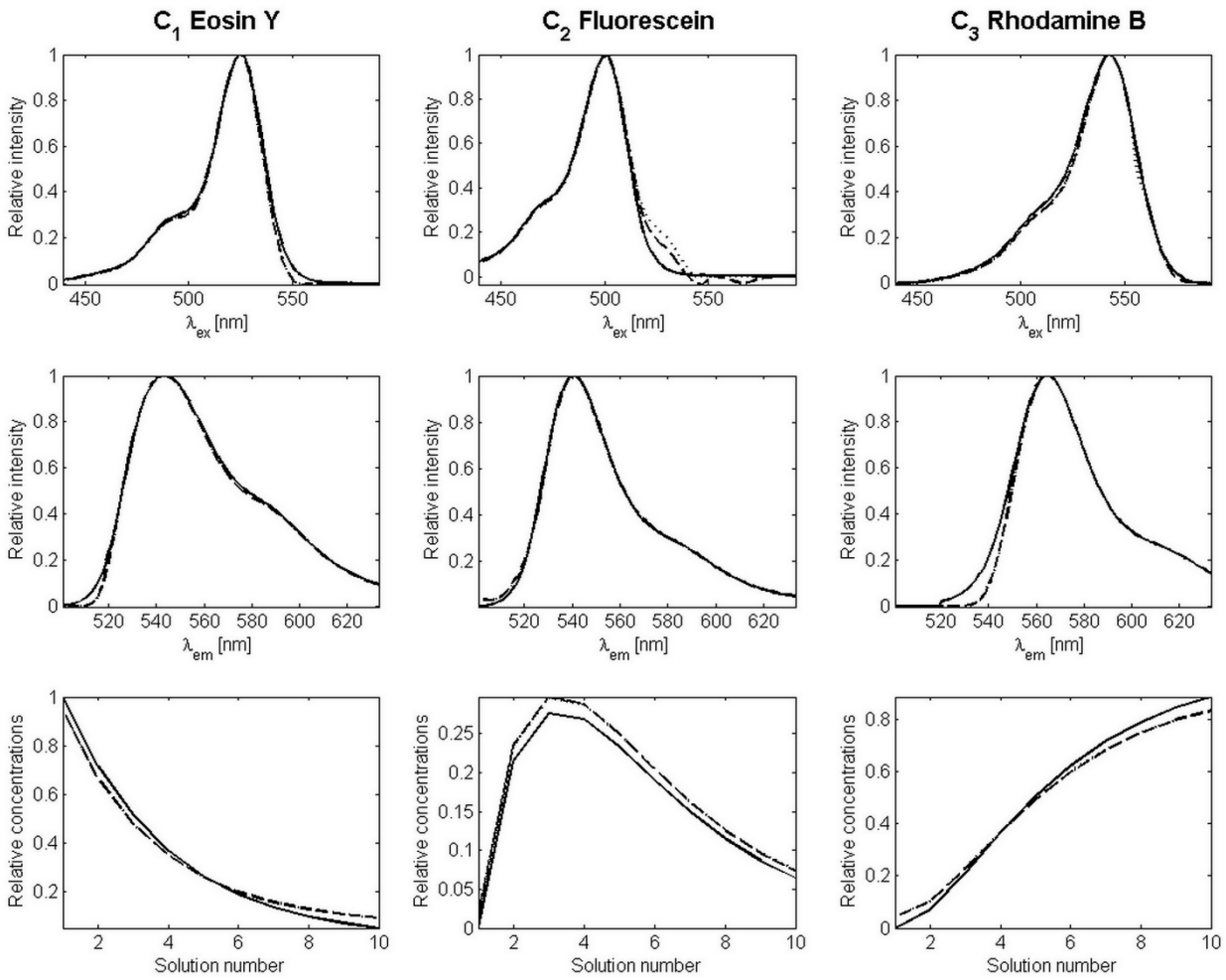
C1 Eosin Y
C2 Fluorescein
C3 Rhodamine B
Relative intensity
λex [nm]
λem [nm]
Relative concentrations
Solution number

Figure 8

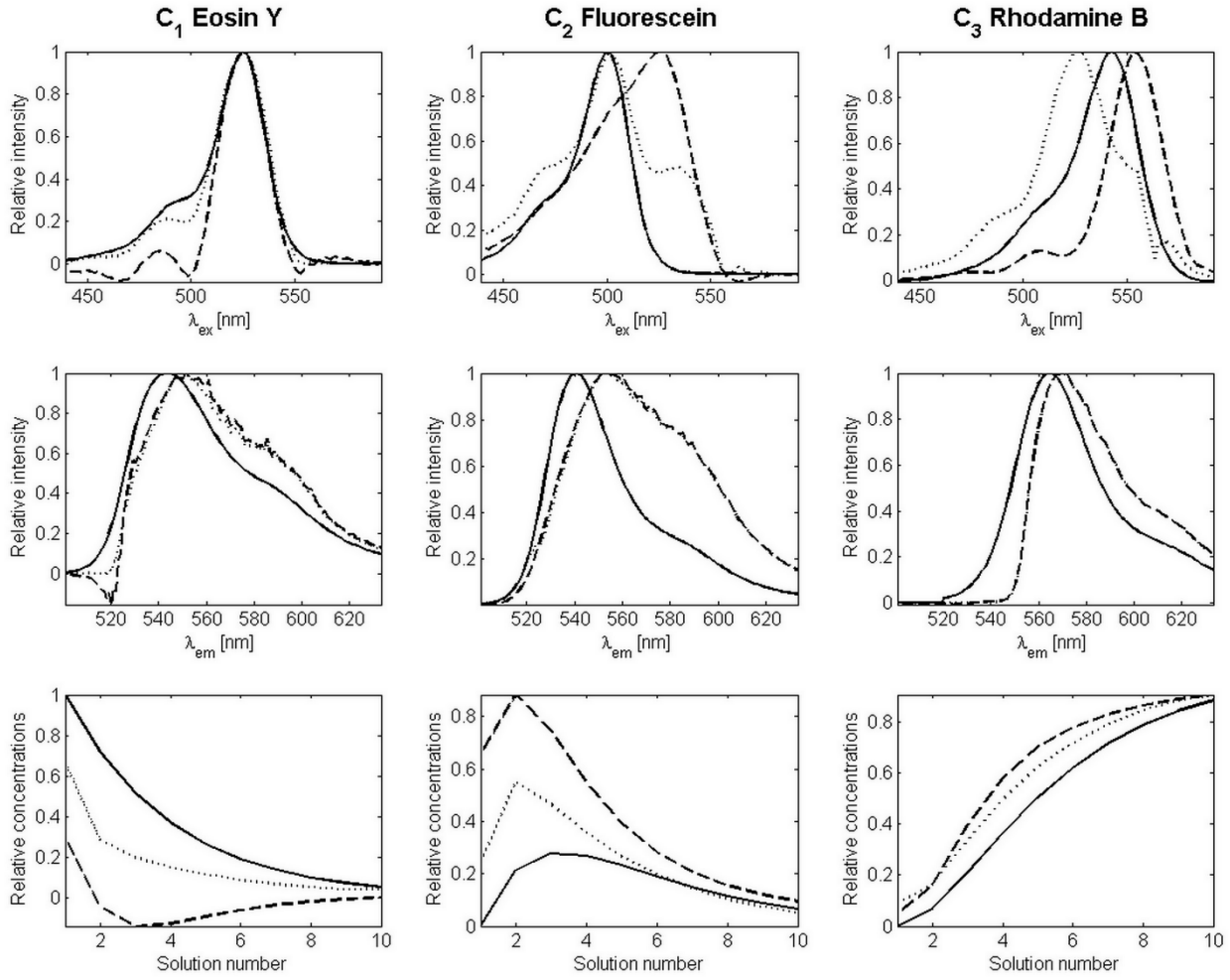
C1 Eosin Y
C2 Fluorescein
C3 Rhodamine B
Relative intensity
λex [nm]
λem [nm]
Relative concentrations
Solution number

Figure 9

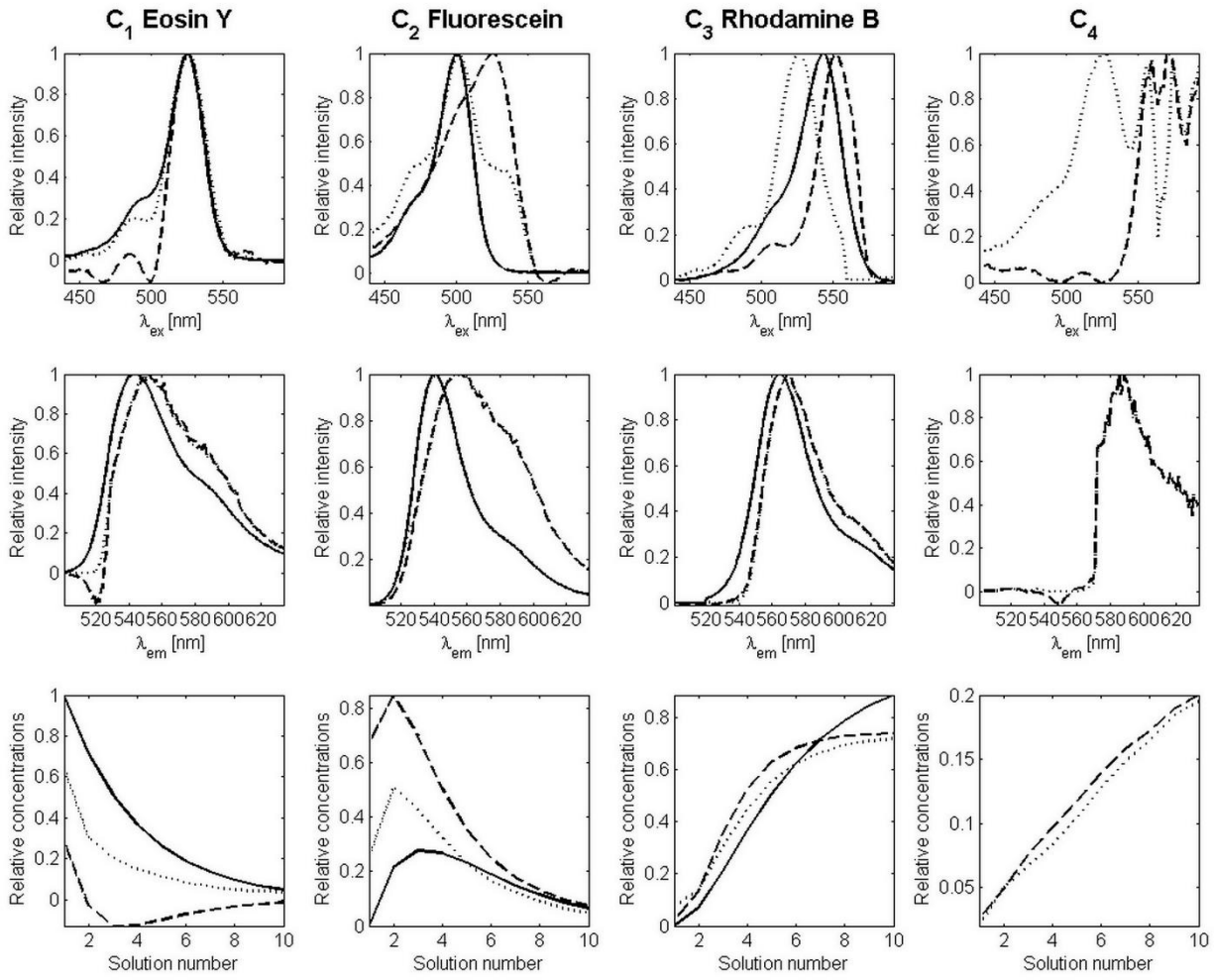
C1 Eosin Y
C2 Fluorescein
C3 Rhodamine B
C4
Relative intensity
λex [nm]
λem [nm]
Relative concentrations
Solution number

Figure 10

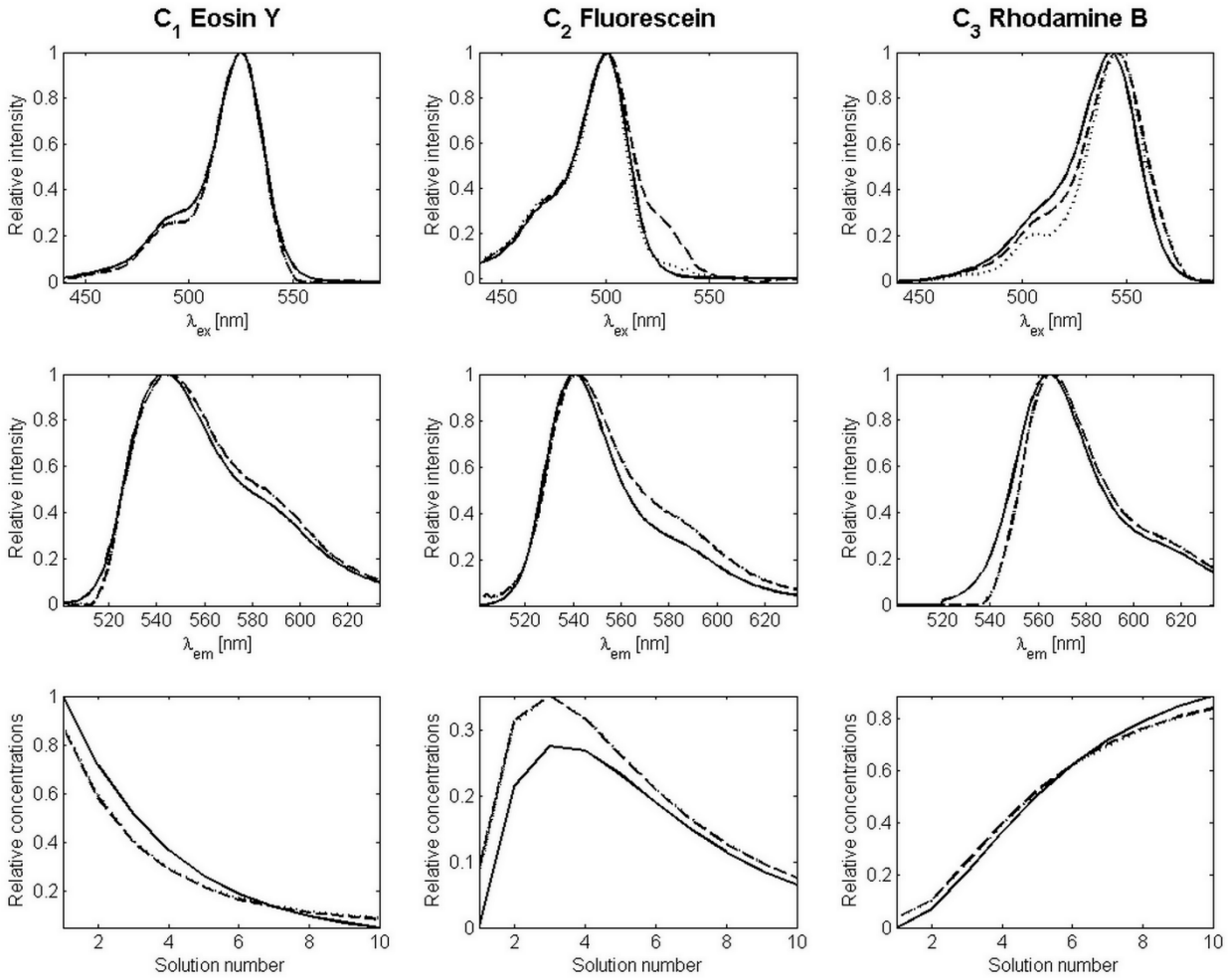
C1 Eosin Y
C2 Fluorescein
C3 Rhodamine B
Relative intensity
λex [nm]
λem [nm]
Relative concentrations
Solution number

Figure 11